1521-0103/356/1/137–147$25.00
THE JOURNAL OF PHARMACOLOGY AND EXPERIMENTAL THERAPEUTICS

http://dx.doi.org/10.1124/jpet.115.227934
J Pharmacol Exp Ther 356:137–147, January 2016

Andrographolide Ameliorates Abdominal Aortic Aneurysm Progression by Inhibiting Inflammatory Cell Infiltration through Downregulation of Cytokine and Integrin Expression

Jun Ren, Zhenjie Liu, Qiwei Wang, Jasmine Giles, Jason Greenberg, Nader Sheibani, K. Craig Kent, and Bo Liu

Division of Vascular Surgery, Department of Surgery (J.R., Z.L., Q.W., J.Gi., J.Gr., K.C.K., B.L.) and Department of Ophthalmology and Visual Sciences (N.S.), University of Wisconsin, Madison, Wisconsin; And Department of Vascular Surgery, 2nd Affiliated Hospital School of Medicine, Zhejiang University, Zhejiang, China (Z.L.)

Received July 21, 2015; accepted October 9, 2015

ABSTRACT

Abdominal aortic aneurysm (AAA), characterized by exuberant inflammation and tissue deterioration, is a common aortic disease associated with a high mortality rate. There is currently no established pharmacological therapy to treat this progressive disease. Andrographolide (Andro), a major bioactive component of the herbaceous plant *Andrographis paniculata*, has been found to exhibit potent anti-inflammatory properties by inhibiting nuclear factor κ-light-chain-enhancer of activated B cells (NF-κB) activity in several disease models. In this study, we investigated the ability of Andro to suppress inflammation associated with aneurysms, and whether it may be used to block the progression of AAA. Whereas diseased aortae continued to expand in the solvent-treated group, daily administration of Andro to mice with small aneurysms significantly attenuated aneurysm growth, as measured by the diminished expansion of aortic diameter (165.68 $\pm$ 15.85% vs. 90.62 $\pm$ 22.91%, $P < 0.05$). Immunohistochemistry analyses revealed that Andro decreased infiltration of monocytes/macrophages and T cells. Mechanistically, Andro inhibited arterial NF-κB activation and reduced the production of proinflammatory cytokines [CCL2, CXCL10, tumor necrosis factor α, and interferon-γ] in the treated aortae. Furthermore, Andro suppressed α4 integrin expression and attenuated the ability of monocytes/macrophages to adhere to activated endothelial cells. These results indicate that Andro suppresses progression of AAA, likely through inhibition of inflammatory cell infiltration via downregulation of NF-κB–mediated cytokine production and α4 integrin expression. Thus, Andro may offer a pharmacological therapy to slow disease progression in patients with small aneurysms.

Introduction

Abdominal aortic aneurysm (AAA), the progressive weakening and dilation of the abdominal aorta, is a major aortic disease associated with a high mortality rate. It occurs most commonly in those over 50 years old, in men, and among those with a family history of the disease (Kent, 2014). As the elderly population increases, AAA becomes a more serious health problem, especially in Western nations. In the United States, the total number of AAAs remains stable at 45,000 cases per year (Dua et al., 2014). The majority of these new cases are small AAAs (defined as less than 5.5- and 5-cm aortic diameter in men and women, respectively) and largely asymptomatic. If left untreated, however, the continuing extension and thinning of the vessel wall may eventually result in a sudden unpredictable rupture. Ruptured AAAs are responsible for at least 13,000 deaths in the United States and 152,000 deaths worldwide annually (Kent, 2014; GBD 2013 Mortality and Causes of Death Collaborators, 2015). Unfortunately, an effective pharmacological treatment of AAAs is not currently available. Moreover, surgical treatment of small aneurysms is not usually recommended due to a low benefit-to-risk ratio. As a result, patients with small aneurysms are left untreated and in a "watchful waiting" program to monitor AAA progression (Filardo et al., 2012; Bown et al., 2013).

The clinical need for effective and safe drugs to slow aneurysm progression in patients with small AAAs has motivated active studies on aneurysm pathophysiology. Intense inflammation, implied by excessive cytokines and massive infiltrated inflammatory cells, is a major pathologic feature of AAAs, which has been replicated in various animal models of AAA (Daugherty and Cassis, 2004; Shimizu et al.,

This study was supported by the National Institutes of Health National Heart, Lung, and Blood Institute [Grant R01HL088447 to B.L.] and the American Heart Association [Grant 15PRE25670074 to J.R.].
dx.doi.org/10.1124/jpet.115.227934.

ABBREVIATIONS: AAA, abdominal aortic aneurysm; Andro, Andrographolide; BSA, bovine serum albumin; DMEM, Dulbecco's modified Eagle's medium; DMSO, dimethylsulfoxide; EC, endothelial cell; FBS, fetal bovine serum; HRP, horseradish peroxidase; IκB, Inhibitor of κB; ICAM-1, intercellular adhesion molecule 1; LPS, lipopolysaccharide; MOMA-2, monocyte + macrophage; NF-κB, nuclear factor κ-light-chain-enhancer of activated B cells; PBS, phosphate-buffered saline; PCR, polymerase chain reaction; RAW, RAW264.7; SMCs, smooth muscle cells; TBS, Tris-buffered saline; TNFα, tumor necrosis factor α; VCAM-1, vascular cell adhesion protein 1.

2006). Therefore, we focused on inflammation in search of a potent antianeurysm strategy.

Andrographis paniculata, also known as Kalmegh (Hindi), Sambiloto (Malay), and Chuanxin Lian (Chinese), is a herbaceous plant in the Acanthaceae family. It has been widely used for treating sore throat, flu, and upper respiratory tract infections in India, Thailand, Malaysia, and China for centuries. Andrographolide (Andro), a major bioactive chemical constituent of the plant, has been demonstrated to have potent anti-inflammatory effects and good tolerance in various disease models, including asthma, stroke, arthritis, restenosis, and myocardial infarction (Wang et al., 2007; Woo et al., 2008; Jayakumar et al., 2013). Data largely from in vitro studies reveal that Andro suppresses inflammation by inhibiting nuclear factor κ-light-chain-enhancer of activated B cells (NF-κB) activity without showing cytotoxicity (Xia et al., 2004; Hsieh et al., 2011).

Since NF-κB activities are elevated in human aneurysmal tissues as well as experimental AAA models (Nakashima et al., 2004), we posit that Andro, through its putative anti–NF-κB properties, may serve as a candidate drug to halt disease progression of small AAAs. Using an elastase-induced murine AAA model, we demonstrate that Andro effectively blocks further aortic expansion and tissue damage of existing aneurysms. Data generated in vivo and in vitro indicate that Andro potently inhibits NF-κB activation and decreases expression of chemokines and cytokines in smooth muscle cells (SMCs) and monocytes/macrophages. Additionally, Andro treatment significantly downregulates α4 integrin expression and subsequently reduces the ability of monocytes/macrophages to adhere to activated endothelial cells.

Materials and Methods

Reagents. Dulbecco's modified Eagle's medium (DMEM) and cell culture reagents were purchased from Gibco Life Technologies (Carlsbad, CA). Andro (≥98% purity, catalog number 365645, lot number MKBL4120V, and lot number MKBS0063V), lipopolysaccharide (LPS) (*Escherichia coli* 0111:B4), and dimethylsulfoxide (DMSO) were purchased from Sigma-Aldrich (St. Louis, MO). Recombinant mouse tumor necrosis factor α (TNFα) was purchased from R&D Systems (Minneapolis, MN). Primary antibodies used include antiphosphorylated p65, anti-p65, anti-Inhibitor of κB (IκB) (Cell Signaling Technology, Danvers, MA), anti–β-actin (Sigma-Aldrich), anti–NF-κB antibody (p65 subunit, active subunit, clone 12H11; Millipore, Boston, MA), anti-CD3 gamma (Epitomics, Burlingame, CA), anti–monocyte + macrophage (MOMA-2), anti–smooth muscle myosin heavy chain 11, anti–smooth muscle α actin (Abcam, Cambridge, MA), and anti-Ly6G (eBioscience, San Diego, CA). Horseradish peroxidase (HRP)–conjugated antibodies were purchased from Bio-Rad (Hercules, CA). Elastin was stained by using a Richard-Allan Scientific Elastic Stain kit (Thermo Fisher Scientific, Rockford, IL). CellTiter-Glo Reagent was purchased from Promega (Madison, WI). Other chemicals and reagents, if not specified, were purchased from Sigma-Aldrich.

Mouse Model of AAA and Administration of Andrographolide. Male C57BL/6J mice, aged 8–12 weeks, underwent AAA induction by elastase perfusion, as described previously (Pyo et al., 2000; Liu et al., 2015; Wang et al., 2015). In brief, after anesthesia, the abdominal aorta was isolated, and the external diameter of the largest portion of the abdominal aorta was measured with a digital caliber. The abdominal aorta was ligated temporarily, then perfused with 0.45 U/ml type I porcine pancreatic elastase (Sigma-Aldrich) or an equal concentration of heat-inactivated (100°C for 15 minutes) elastase (control) for 5 minutes at a constant pressure of 100 mm Hg. After perfusion, the aortotomy and abdominal incisions were closed. The mouse was kept on a warming pad until fully recovered from anesthesia. Seven days after aneurysm induction, mice were randomly assigned to two groups: (1) solvent (DMSO) control and (2) Andro. Immediately prior to i.p. injection, 3 μl of Andro (dissolved in DMSO at 50 mg/ml) was diluted with 200 μl of saline. An equal volume of DMSO was diluted and injected accordingly. We chose postoperative day 7 to begin treatment because aneurysmal dilations at this time are small but significant (Supplemental Fig. 1, A and B) (Miyake et al., 2007; Liu et al., 2014). Daily i.p. injection of DMSO to mice produced an insignificant effect on aneurysmal dilation compared with mice not receiving DMSO (165.68 ± 15.85% vs. 166.67 ± 15.46%, $P > 0.05$ in elastase-treated arteries postoperative at day 14; and 43.54 ± 7.24% vs. 43.62 ± 3.56%, $P > 0.05$ in inactive elastase-treated arteries postoperative at day 14). The in vivo dosage of Andro in the literature ranges from 1 to 100 mg/kg body weight, with 5 mg/kg body weight (used in the current study) as a commonly used dosage, which is considerably lower than the LD_{50} for intraperitoneally administered andrographolide (11.6 g/kg body weight) (Handa and Sharma, 1990; Wang et al., 2007; Hsieh et al., 2011; Zhu et al., 2013). At the selected time points, mice were euthanized by CO_2 inhalation. The external diameter of the largest portion of abdominal aortas was measured and used to calculate the percentage increase in maximal external aortic diameter compared to the diameter recorded prior to the elastase perfusion. Tissues intended for RNA isolation were harvested and stored in RNAlater RNA Stabilization Reagent (Qiagen, Valencia, CA). Tissues intended for immunohistochemistry were imbedded in O.C.T. Compound (Sakura, Alphen aan den Rijn, Netherlands). Frozen sections were cut to 6 μm thick using a Leica CM3050S cryostat (Buffalo Grove, IL). All animal experiments in this study were approved by the Institutional Animal Care and Use Committee of the University of Wisconsin–Madison (protocol M02284) and performed in accordance with the Guide for the Care and Use of Laboratory Animals published by the U.S. National Institutes of Health (National Research Council, 2011).

Cell Culture and In Vitro Treatment. Primary mouse aortic SMCs were isolated from arteries of C57BL/6J mice as previously described (Clowes et al., 1989; Lengfeld et al., 2012). Primary SMCs were grown at 37°C in 5% CO_2 in DMEM modified to contain 4 mM L-glutamine, 1 g/l D-glucose, and 110 mg/l sodium pyruvate (Life Technologies) supplemented with 10% fetal bovine serum (FBS), 100 U/ml penicillin, and 100 U/ml streptomycin. Cells between passages three and seven were used. The mouse monocyte/macrophage cell line RAW264.7 (RAW) was obtained from American Type Culture Collection (Manassas, VA) and was maintained as recommended in DMEM modified containing 4.5 g/l D-glucose (Life Technologies) supplemented with 10% FBS, 100 U/ml penicillin, and 100 U/ml streptomycin. Mouse aortic endothelial cells (ECs) were isolated from male C57BL/6J mice, as described previously (Su et al., 2003). ECs were grown on 1% gelatin-coated dishes in DMEM containing 20% FBS, 2 mM L-glutamine, 2 mM sodium pyruvate, 20 mM HEPES, 1% nonessential amino acids, 100 μg/ml streptomycin, 100 U/ml penicillin, freshly added heparin at 55 U/ml (Sigma-Aldrich), 100 μg/ml endothelial growth supplement (Sigma-Aldrich), and murine recombinant interferon-γ (R&D Systems) at 44 U/ml (Su et al., 2003). For in vitro treatment, a stock solution of 15 mM was prepared by dissolving Andro in DMSO, then diluted to desired concentrations with medium immediately prior to experiments. The final concentration of DMSO was 0.1%, which showed no effects by itself (Fig. 5, B–E; Supplemental Figs. 2, A–G and 3, A–G). Andro, at the final concentration of 15 μM, has been reported to effectively inhibit NF-κB in ECs and SMCs (Xia et al., 2004; Ren et al., 2014), whereas the dosage of Andro for treating macrophages is less established. To determine the in vitro dosage, we conducted dose-response studies using RAWs. Andro did not significantly decrease cell viability below a dose of 30 μM (Supplemental Fig. 4A). Preincubation of RAWs with 15 or 20 μM Andro reduced adhesion to the fibronectin-coated surface by 70 and 80%, respectively. However, differences in adhesion inhibition caused by 15 and 20 μM did not reach significance (Supplemental Fig. 4B), suggesting 15 μM Andro

caused close-to-maximal inhibition on adhesion of monocytes/macrophages without affecting viability. Therefore, we conducted the rest of the in vitro studies with 15 μM Andro.

RNA Isolation and Quantitative Real-Time Polymerase Chain Reaction. Total RNA was extracted from cultured cells or mouse aortic arteries using Trizol reagent (Life Technologies) according to the manufacturer's protocols. Two micrograms of RNA was used for the first-strand cDNA synthesis (Applied Biosystems, Carlsbad, CA). A no-reverse-transcriptase control was included in the same polymerase chain reaction (PCR) mixtures without reverse transcriptase to confirm the absence of DNA contamination in RNA samples. The quantitative real-time PCR primers for *Ccl2*, *Ccl5*, *Ccl7*, *Ccl10*, *Ccl16*, *Tnf*, *Ifng*, and *Gapdh* were purchased from Qiagen. Primers for amplification of integrins were *Itga4* (forward: 5′ GAATCCAAACCAGACCTGCGA 3′; reverse: 5′ TGACGTAGCAAATGCCAGTGG 3′), *ItgaL* (forward: 5′ ATGCACCAAGTACAAAGTCAGC 3′; reverse: 5′ TTGGTCGAACTCAGGATTAGC 3′), *Itgb1* (forward: 5′ TTCAGACTTCCGCATTGGCTTTGG 3′; reverse: 5′ TGGGCTGGTGCAGTTTTGTTCAC 3′), and *Itgb2* (forward: 5′ CAGGAATGCACCAAGTACAAAGT 3′; reverse: 5′ CCTGGTCCAGTGAAGTTCAGC 3′) (Ip et al., 2007). Reactions were carried out in 96-well optical reaction plates using SYBR Green PCR Master Mix (Applied Biosystems) with gene-specific primers in a 7500 Fast Real-Time PCR System (Applied Biosystems). Amplification of each sample was analyzed by melting curve analysis, and relative differences in each PCR sample were corrected using glyceraldehyde-3-phosphate dehydrogenase mRNA as an endogenous control, and were normalized to the level of control by using the $2^{-\Delta\Delta Ct}$ method. $\Delta\Delta Ct = \Delta Ct(test) - \Delta Ct(control)$, whereas $\Delta Ct = Ct(target\ gene) - Ct(endogenous\ control)$. (Si et al., 2012).

CellTiter-Glo Luminescent Cell Viability Assay. RAWs were seeded in 96-well plates at a density of 3×10^4 cells per well. Twenty-four hours later, the medium was replaced with fresh growth medium containing Andro or DMSO. After culturing for 48 hours, CellTiter-Glo Reagent was added. Luminescence was recorded 10 minutes after reagent addition using a FlexStation 3 Microplate Reader (Molecular Devices, Sunnyvale, CA).

Cell Adhesion Assay. Adhesion to a fibronectin-coated surface was evaluated in 96-well plates as described previously (Liu et al., 2015). In brief, RAWs pretreated with Andro or DMSO were seeded in fibronectin-coated wells and incubated at 37°C for 45 minutes. After three washes with phosphate-buffered saline (PBS), cells were fixed in 4% paraformaldehyde, then stained with crystal violet (5 mg/ml in 2% ethanol) for 10 minutes. Wells were washed three times with PBS, then turned upside down to dry completely. After adding 2% SDS to each well and incubating for 30 minutes, plates were read at 550 nm using a FlexStation 3 Microplate Reader (Molecular Devices).

Monocyte-Endothelial Cell Interaction. A monolayer of ECs was grown on a 1% gelatin-coated 24-well plate. To visualize cell adhesion, RAWs were fluorescently labeled with the CellTracker Green CMFDA Dye (Life Technologies) prior to adding the cells to ECs. ECs were activated with TNFα (10 ng/ml) for 12 hours with or without Andro (15 μM) pretreatment, whereas RAWs were only preincubated with Andro or DMSO for 12 hours. After incubating RAWs with ECs for 20 minutes, loosely adherent cells were shaken off followed by three washes with PBS. Six fields were randomly chosen, and adherent cells were photographed by fluorescence microscopy (Nikon DS-Ri1; Nikon Instruments, Melville, NY). The number of adherent cells was counted using ImageJ (National Institutes of Health, Bethesda, MD), and data are expressed as the mean number of counted cells/field ± S.E.M.

Immunoblotting. Cells were lysed in radio-immunoprecipitation assay buffer (Sigma-Aldrich), and total protein was extracted. Equal amounts of protein extract were separated by SDS-PAGE and transferred to polyvinylidene difluoride membranes. The membranes were then incubated with primary antibody followed by HRP-labeled goat anti-rabbit or anti-mouse immunoglobulin G (Bio-Rad). Labeled proteins were visualized with an enhanced chemiluminescence system (Thermo Fisher Scientific). For quantification, optical density of secreted proteins, determined by ImageJ, was normalized to the loading control density.

Immunohistochemistry. Tissue sections were permeabilized with 0.1% Triton X-100 in Tris-buffered saline (TBS) for 10 minutes at room temperature. Nonspecific sites were blocked using 5% bovine serum albumin (BSA) and 10% normal donkey serum in TBS for 2 hours at room temperature. Primary antibodies diluted in TBS with 5% BSA were then applied to arterial sections and incubated overnight at 4°C. The next day, arterial sections were rinsed with TBS plus 0.025% Triton X-100, followed by incubation with HRP- or fluorophore-conjugated secondary antibodies diluted in TBS with 1% BSA for 1 hour at room temperature. After 3,3-diaminobenzidine development and counterstaining with hematoxylin or 4′,6-diamidino-2-phenylindole for immunofluorescence staining, stained tissue sections were visualized with a Nikon Eclipse Ti inverted microscope system, and digital images were acquired using a Nikon DS-Ri1 digital camera. Quantification of stains was performed with ImageJ software as previously described.

Statistical Analysis. Student's t test or one-way analysis of variance with Bonferroni's post-hoc test was used to evaluate the statistical differences. All experiments were repeated at least three times. Data are presented as the mean ± S.E.M. Differences with $P < 0.05$ were considered significant.

Results

Andrographolide Inhibits Progression of Abdominal Aortic Aneurysm. We tested Andro in a murine model of AAA, which used a brief (5 minutes) intraluminal perfusion of the abdominal aorta with porcine pancreas elastase. The control mice were subjected to identical surgical manipulation, but were perfused with heat-inactivated elastase. With time, the elastase-treated group exhibited continuous aortic expansion (Supplemental Fig. 1, A and B), which was accompanied by the appearance of typical aneurysmal pathologic features, including inflammation infiltration, SMC depletion, and elastin degradation (Liu et al., 2014, 2015; Wang et al., 2015). In contrast, aorta treated with inactivated elastase showed neither continuous aortic expansion nor tissue deterioration (Supplemental Fig. 1, A and B).

To evaluate the therapeutic potential of Andro, we selected day 7 post elastase perfusion as the starting point for drug treatment. At this time point, the aortic expansion was small but significantly larger than arteries perfused with inactivated elastase (Supplemental Fig. 1, A and B). Furthermore, inflammation as measured by monocyte and macrophage accumulation in the aortic tissue had clearly developed (Liu et al., 2015). The elastase-treated mice were randomly divided into two groups, one treated daily with solvent (DMSO) and the other with Andro (5 mg/kg body weight) (Fig. 1A). A separate group of mice that were perfused with inactivated elastase and then treated with solvent were used as a baseline control. Mice were sacrificed 14 days post aneurysm induction. Elastase-perfused solvent-treated aortae predominantly appeared dilated and inflamed, whereas elastase-perfused Andro-treated aortae appeared normal, which resembled arteries perfused with inactivated elastase (Fig. 1B). We quantified the inhibitory effects of Andro on aortic dilation by calculating the percentage increase in maximum aortic diameter. As shown in Fig. 1B, Andro markedly decreased the aortic expansion compared with the solvent-treated mice (90.62 ± 22.91% vs. 165.68 ± 15.85%, $P < 0.05$). Histologically, administration of Andro preserved vascular tissue

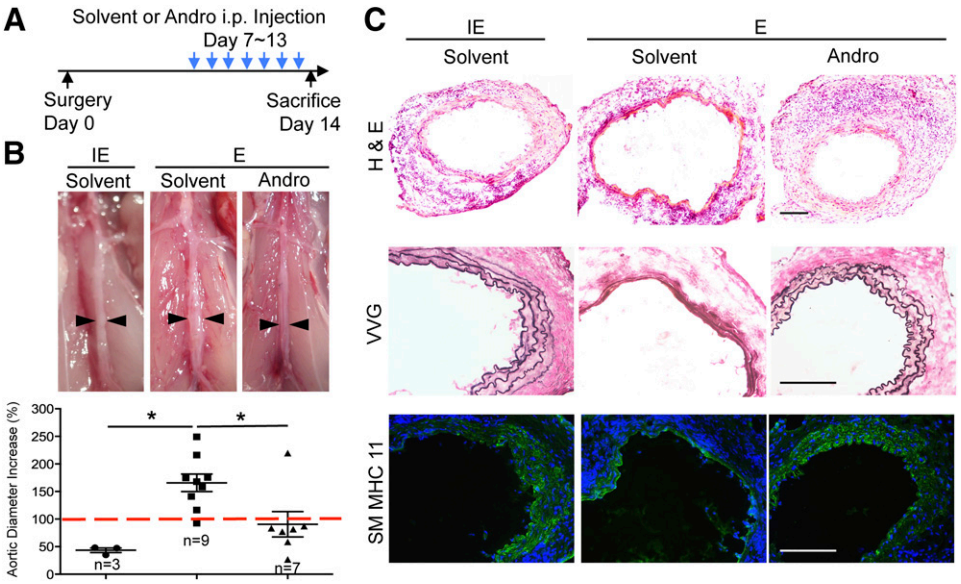

Fig. 1. Andro inhibits progression of small AAAs. (A) Schematic diagram of Andro treatment in mice. (B) Representative photos and aortic expansion of Andro- and solvent-treated mice, taken 14 days after surgery. E, elastase; IE, inactivated elastase. An AAA is defined as a percentage increase in aortic diameter that is equal to or greater than 100% (red dashed line). All values represent the mean ± S.E.M. (n = 3–9; $^*P < 0.05$, one-way analysis of variance). (C) Representative images of arterial sections stained with H&E, Verhoeff–Van Gieson (VVG), and smooth muscle myosin heavy chain 11 (SM MHC 11; green) overlaid with 4′,6-diamidino-2-phenylindole (blue). Arteries were harvested 14 days after surgery. Scale bar = 200 μm.

integrity. It reduced the tissue damage, elastin degradation, and loss of SMCs (Fig. 1C).

Andrographolide Inhibits NF-κB Activation during AAA Pathogenesis. Since Andro has been implicated to act on the NF-κB pathway, we investigated whether Andro affects NF-κB activation in aneurysm using an antibody that recognizes the DNA-binding or activated form of p65 (Aoki et al., 2007). Prior to Andro treatment, activated p65 was readily detectable in the aortic wall 7 days after elastase perfusion, mostly in cells that were positive for smooth muscle α actin (an SMC marker) as well as in cells positive for MOMA-2 (a monocyte and macrophage marker) (Fig. 2, A and B). Activation of NF-κB persisted in the aortic wall for at least 14 days post aneurysm induction (Fig. 2C). The 1-week Andro treatment (days 7–13) nearly eliminated NF-κB activation (Fig. 2C).

Andrographolide Attenuates AAA-Associated Inflammatory Cytokine Expression. To further investigate how Andro halts aneurysm progression, we turned to cultured SMCs and macrophages, two primary sources of inflammatory cytokine during AAA pathogenesis. To mimic inflammation associated with AAA, we treated SMCs isolated from the mouse aorta with TNFα (10 ng/ml), which caused a rapid and sustained phosphorylation of p65 at Ser536 as well as degradation of IκB (Fig. 3, A and B). Pretreating SMCs with Andro (15 μM) greatly attenuated p65 phosphorylation but did not significantly alter IκB degradation (Fig. 3, A and B). Next, we examined whether Andro inhibits the expression of NF-κB target genes (in this case, chemokines and cytokines found in aneurysmal tissues). As shown in Fig. 3, C–H, TNFα stimulated expression of *Ccl2, Ccl5, Ccl7, Cxcl10, Cxcl16*, and *Tnf* in SMCs, ranging from 10- to 160-fold. Compared with DMSO, Andro significantly decreased production of these inflammatory cytokines (Fig. 3, C–H). Interestingly, expression of *Ifng* in SMCs was not affected by TNFα or Andro treatment (Fig. 3I).

Although Andro effectively blocked basal levels of cytokine and chemokine expression in RAWs, this monocyte/macrophage cell line was not as responsive to TNFα (10 ng/ml) as SMCs (Supplemental Fig. 5, A–G). Since toll-like receptor signaling plays a crucial role in pathogenesis of aneurysms (Vorkapic et al., 2015), we used the well characterized toll-like receptor ligand LPS (100 ng/ml) as a stimulus. Andro decreased LPS-induced p65 phosphorylation at Ser536 without affecting IκB in RAWs (Fig. 4, A and B). Moreover, Andro reduced the LPS-induced expression of *Ccl2*, *Ccl5*, *Ccl7*, *Cxcl10*, and *Tnf* by 40–80% (Fig. 4, C–F and H). Of note, expression of *Cxcl16* and *Ifng* in RAWs was not sensitive to LPS, even though Andro decreased basal levels of these inflammatory cytokines (Fig. 4, G and I).

Andrographolide Decreases Monocyte/Macrophage Adhesion. Firm adhesion of monocytes/macrophages to the endothelium is another crucial event leading to vascular inflammation. To simulate this early inflammatory step, we used an in vitro adhesion assay in which fluorescence-labeled RAWs were allowed to adhere to a monolayer of ECs for 20 minutes. After washing vigorously, adhered RAWs were imaged and counted. Activation of ECs with TNFα (10 ng/ml) increased the number of adhered RAWs by 130% (Fig. 5A). Pretreating ECs, RAWs, or both cell types with Andro resulted in significantly reduced adhesion of RAWs. However, treating RAWs or both cell types with Andro produced more profound inhibition than treating EC alone (Fig. 5A).

NF-κB is known to regulate endothelial expression of adhesion molecules, including vascular cell adhesion molecule 1 (VCAM-1) and intercellular adhesion molecule 1 (ICAM-1) (Wang et al., 2007). In comparison, the underlying mechanism of Andro on macrophage adhesion is less understood. Very late antigen 4 (also known as α4β1 integrin) and lymphocyte function–associated antigen 1 (also known as αLβ2 integrin) are major integrins on the monocyte/macrophage surface that interact with VCAM-1 and ICAM-1 during adhesion. Therefore, we tested whether Andro affects integrin expression in RAWs. As shown in Fig. 5B, treatment of RAWs with Andro for 6 or 12 hours reduced α4 (*Itga4*) integrin expression by 57 and 58%. The expression of β1 (*Itgb1*), αL (*Itgal*), and β2 (*Itgb2*) integrins were not significantly affected (Fig. 5, C–E).

Andrographolide Inhibits Inflammatory Cytokine Production and Inflammatory Cell Infiltration in Aneurysm. Having established the inhibitory role of Andro in cultured SMCs and macrophages, we re-examined mouse

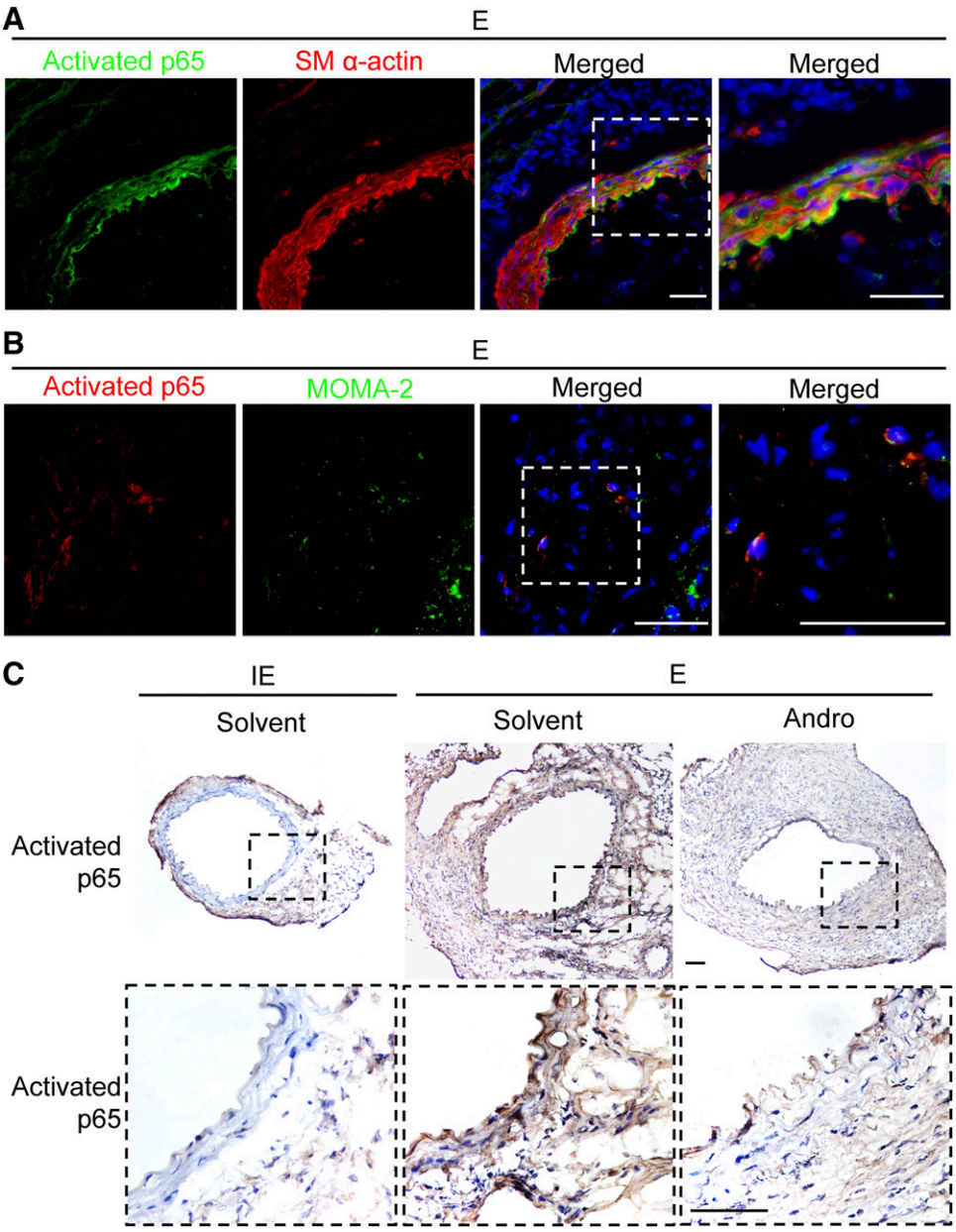

Fig. 2. Andro attenuates NF-κB activation in aortic tissues. (A and B) Representative images of arterial sections coimmunostained for activated p65 (green) and smooth muscle α-actin (smooth muscle α-actin; red) (A) or activated p65 (red) and MOMA-2)green) (B) overlaid with 4′,6-diamidino-2-phenylindole (blue). Areas highlighted by white dashed boxes are shown at higher magnification on the right. Arteries were harvested 7 days after elastase perfusion. Scale bar = 50 μm. (C) Representative images of arterial sections immunohistochemically stained for activated p65. E, elastase; IE, inactivated elastase. Areas highlighted by black dashed boxes are shown at higher magnification at the bottom. Arteries were harvested 14 days after elastase perfusion. Scale bar = 100 μm.

aneurysm tissues. Consistent with the literature, expression of AAA-associated inflammatory cytokines, including *Tnf, Ifng, Ccl2, Ccl5, Ccl7*, *Cxcl10*, and *Cxcl16*, was greatly increased in the elastase-perfused arterial wall as compared with heat-inactivated elastase-treated arteries (Fig. 6, A–G). Daily administration of Andro 7 days after aneurysm induction significantly inhibited expression of *Ccl2*, *Cxcl10*, *Tnf*, and *Ifng* as compared with solvent treatment (Fig. 6, A–D). Interestingly, *Ccl5*, *Ccl7*, and *Cxcl16* mRNA expression was not significantly affected by Andro treatment (Fig. 6, E–G).

We next examined vascular infiltration of inflammatory cells. Immunohistochemistry with antibodies against MOMA-2 (a monocyte and macrophage maker), CD3 (a T cell marker), and Ly6G (a neutrophil marker) revealed that infiltration of monocytes/macrophages as well as T cells were significantly decreased by Andro treatment (Fig. 7, A and B). The number of Ly6G+ cells were comparable between Andro and solvent treatment groups. Of note, at day 14 after aneurysm induction, Ly6G+ cells constituted less than 1% of arterial wall cells (Fig. 7, A and B).

Discussion

Chronic inflammation has long been recognized as a crucial pathologic event in AAAs. However, its underlying molecular and cellular mechanisms remain incompletely understood. Experimental evidence published by several investigative groups, including our own, suggests active interplays between infiltrating macrophages and resident SMCs (Curci and Thompson, 2004; Liu et al., 2015). Vascular SMCs are a major source of extracellular matrix proteins that render elastic property and tensile strength to the aortic wall. On the other hand, injured SMCs actively recruit inflammatory cells by producing chemokines. If SMCs are considered as the soil of inflammation, the recruited inflammatory cells, particularly M1 macrophages, are inflammatory amplifiers and tissue

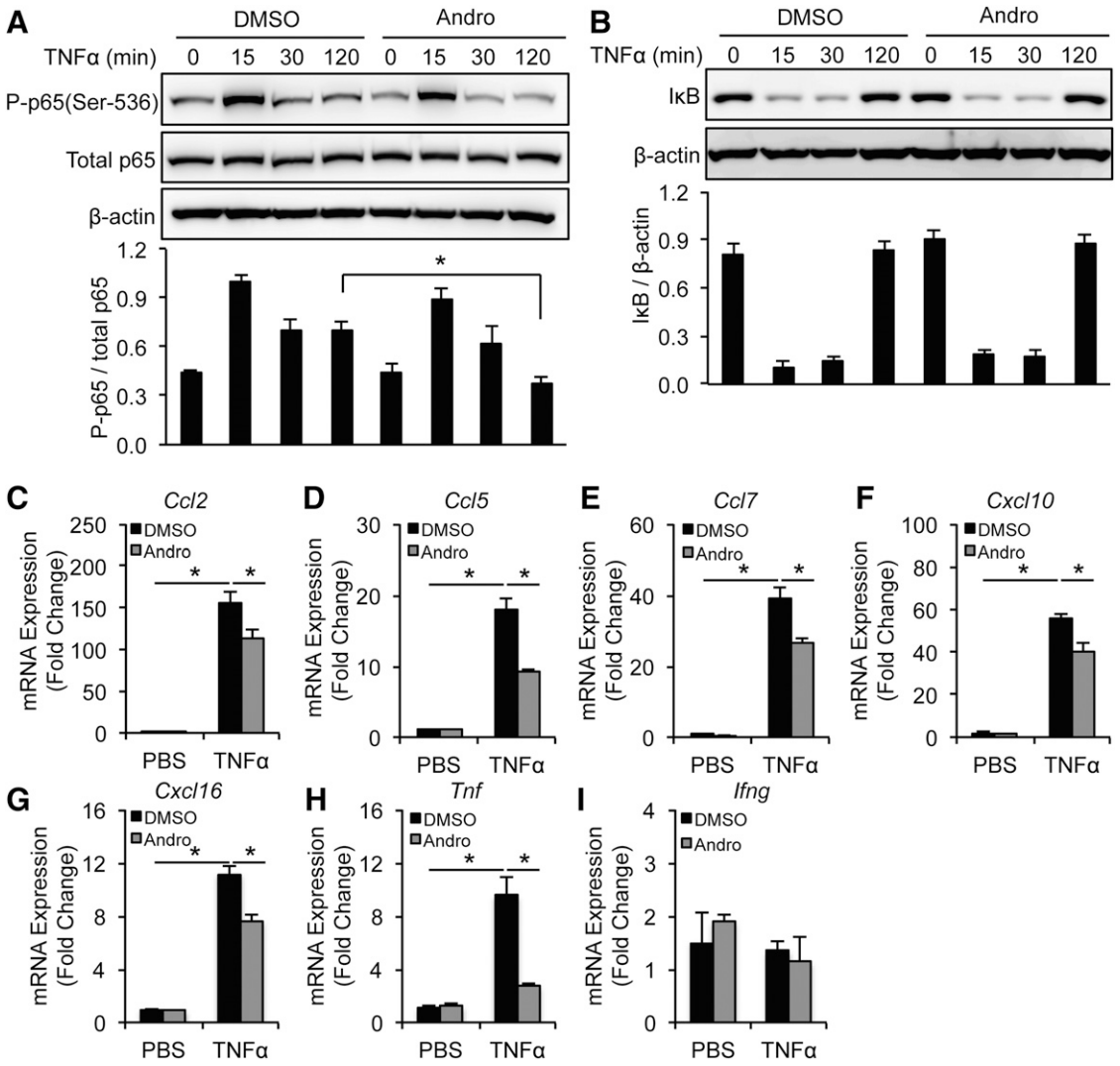

Fig. 3. Andro inhibits NF-κB activation and cytokine expression in TNFα-treated SMCs. (A and B) SMCs were pretreated with solvent (DMSO) or Andro (15 μM) for 1 hour before incubation with TNFα (10 ng/ml) for the indicated times. Whole-cell lysates were subjected to immunoblotting analysis with indicated antibodies. (C–I) SMCs were pretreated with solvent (DMSO) or Andro (15 μM) for 1 hour before incubation with TNFα (10 ng/ml) for 6 hours. mRNA expression of inflammatory chemokines and cytokines was analyzed by quantitative real-time PCR. All values represent the mean ± S.E.M. (n = 3–6; $^*P < 0.05$, one-way analysis of variance (A–I). P-p65, phosphorylated p65.

destroyers. They amplify inflammation by releasing cytokines (Curci and Thompson, 2004), destroy tissues by producing matrix-degrading enzymes such as matrix metalloproteinases (Thompson et al., 1995; Longo et al., 2002), and eliminate SMCs through proapoptotic or necrotic signals, including reactive oxygen species, TNFα, and Fas ligand (Li et al., 1997; Wang et al., 2014). As such, anti-inflammatory strategies, including those that deplete neutrophils or neutralize cytokines, such as TNFα, preserve smooth muscle and reduce matrix proteolysis (Eliason et al., 2005; Jayaraman et al., 2008). Evidence presented here proved that inhibition of inflammation through systematic administration of Andro blocked aneurysm progression in mice, evidenced by halted aortic expansion, reduced elastin degradation, preserved medial SMCs, and reduced number of infiltrating monocytes, macrophages, and T lymphocytes.

Among the Andro-sensitive chemokines/cytokines, CCL2, also called monocyte chemoattractant protein-1, is well known for its role in inflammatory recruitment in aneurysm. Targeted gene deletion of *Ccl2* or its receptor *Ccr2* confers aneurysm resistance (MacTaggart et al., 2007; Aoki et al., 2009; Moehle et al., 2011). In this study, Andro potently reduced the *Ccl2* mRNA accumulation in the aortic wall by 93.18% compared with the solvent control. Andro also decreased the local expression of other established proinflammatory cytokines, including *Tnf*, *Ifng,* and *Cxcl10*. Inhibition of cytokine expression by Andro was replicated to a large extent in cultured aortic SMCs, as well as in a monocyte/macrophage cell line RAWs. Of note, inhibition of certain chemokines, such as *Ccl2*, *Ccl7*, and *Cxcl10*, was more profound in RAWs than in SMCs (80–95% vs. 25–30%). Since Andro produced a similar reduction in p65 phosphorylation in these two cell types, we speculate that the differential response reflects a cell-type-dependent transcription regulation of chemokines. Regulation of gene expression is a complex process requiring coordination of multiple transcription factors and coactivators, which is frequently controlled by epigenetic modifications. It is possible that NF-κB plays a

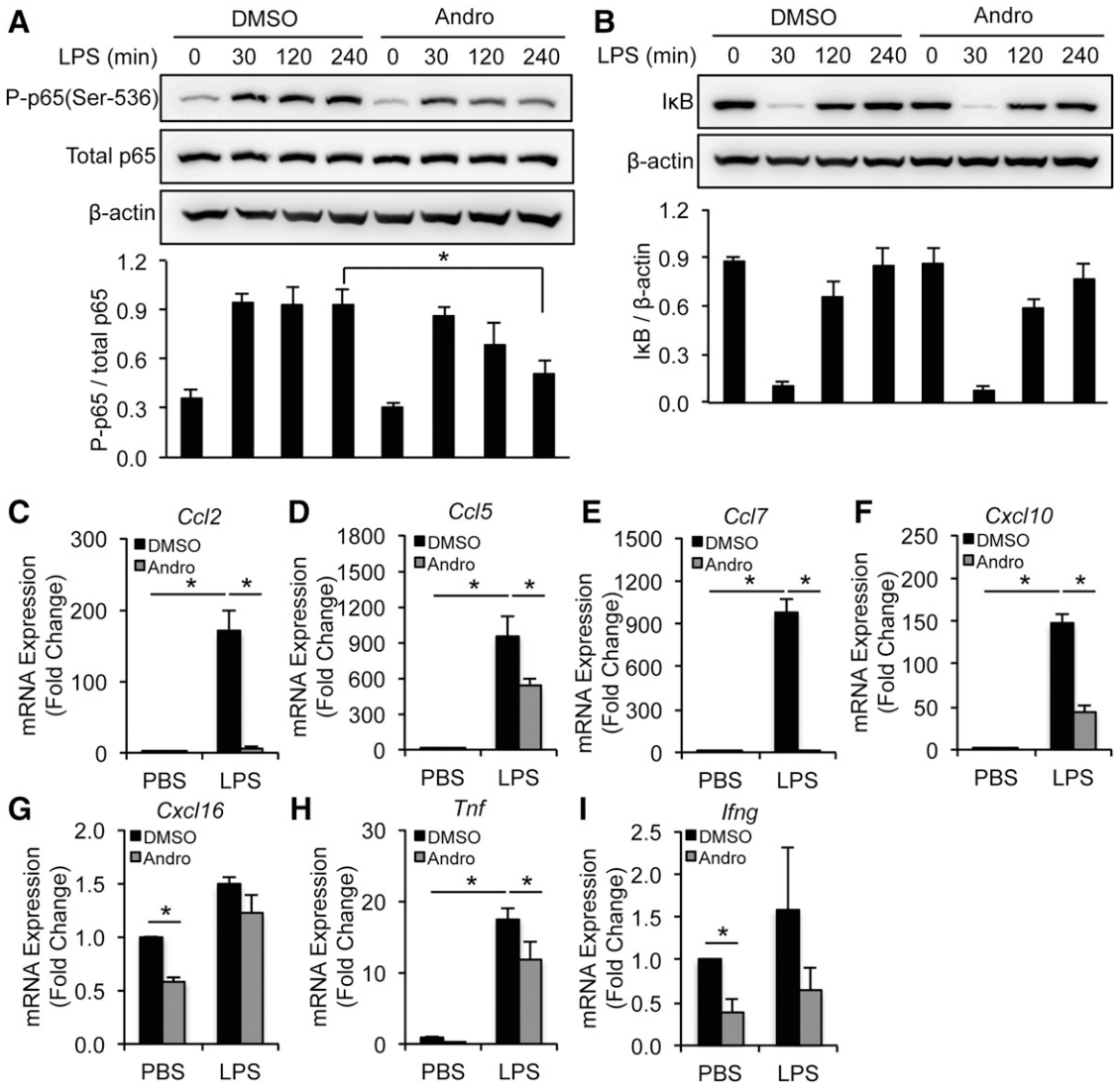

Fig. 4. Andro inhibits NF-κB activation and cytokine expression in LPS-treated monocytes/macrophages. (A and B) RAW264.7 cells were pretreated with solvent (DMSO) or Andro (15 μM) for 1 hour before incubation with LPS (100 ng/ml) for the indicated times. Whole-cell lysates were subjected to immunoblotting analysis with indicated antibodies. (C–I) RAW264.7 cells were pretreated with solvent (DMSO) or Andro (15 μM) for 1 hour before incubation with LPS (100 ng/ml) for 6 hours. mRNA expression of inflammatory chemokines and cytokines was analyzed by quantitative real-time PCR. All values represent the mean ± S.E.M. [$n = 4–5$; *$P < 0.05$, one-way analysis of variance (A–F and H) and two-tailed Student's t test (G and I)]. P-p65, phosphorylated p65.

more dominant regulatory role in chemokine transcription in monocytes/macrophages than in SMCs. However, this potential mechanism needs to be experimentally tested.

Our data revealed a novel function of Andro, i.e., inhibition of leukocyte adhesion. Aside from the reported inhibitory effect of Andro on expression of ICAM-1, VCAM-1, and E-selectin in ECs (Jiang et al., 2007; Wang et al., 2007; Lu et al., 2014), the present study demonstrated that Andro inhibited the expression of α4 integrin in monocytes/macrophages. To the best of our knowledge, this is the first demonstration that Andro inhibited the α4 integrin expression and endothelium adhesion of monocytes/macrophages. Interestingly, in the in vitro monocyte-endothelial cell interaction study, we found that pretreating RAWs with Andro (15 μM) produced a far more inhibitory effect on adhesion than pretreating endothelial cells.

In dose-response studies, Andro did not significantly decrease the viability of RAWs until it reached 30 μM. Preincubation of RAWs with 15 and 20 μM Andro reduced adhesion ability, but not viability, to the fibronectin-coated surface by 70 and 80%, respectively. However, differences in adhesion inhibition caused by these two doses of Andro did not reach significance, suggesting that Andro at 15 μM caused close-to-maximal inhibition of monocyte/macrophage adhesion. This observation is somewhat different from a prior study, which showed that 20 and 50 μM Andro dose-dependently suppressed NF-κB activity by 16.4 and 55.6%, respectively. However, neither concentration diminished cell viability, as measured by 3-(4,5-dimethylthiazol-2-yl)-2,5-diphenyltetrazolium bromide assay (Hsieh et al., 2011). It is possible that monocytes and macrophages are more sensitive to Ando or NF-κB inhibition. However, further experimental evidence is needed to confirm this possibility.

At the molecular level, we showed that Andro significantly decreased aortic activity of NF-κB. Whereas IκB degradation constitutes a canonical regulatory step for NF-κB activation (Oeckinghaus and Ghosh, 2009; Ren et al., 2014),

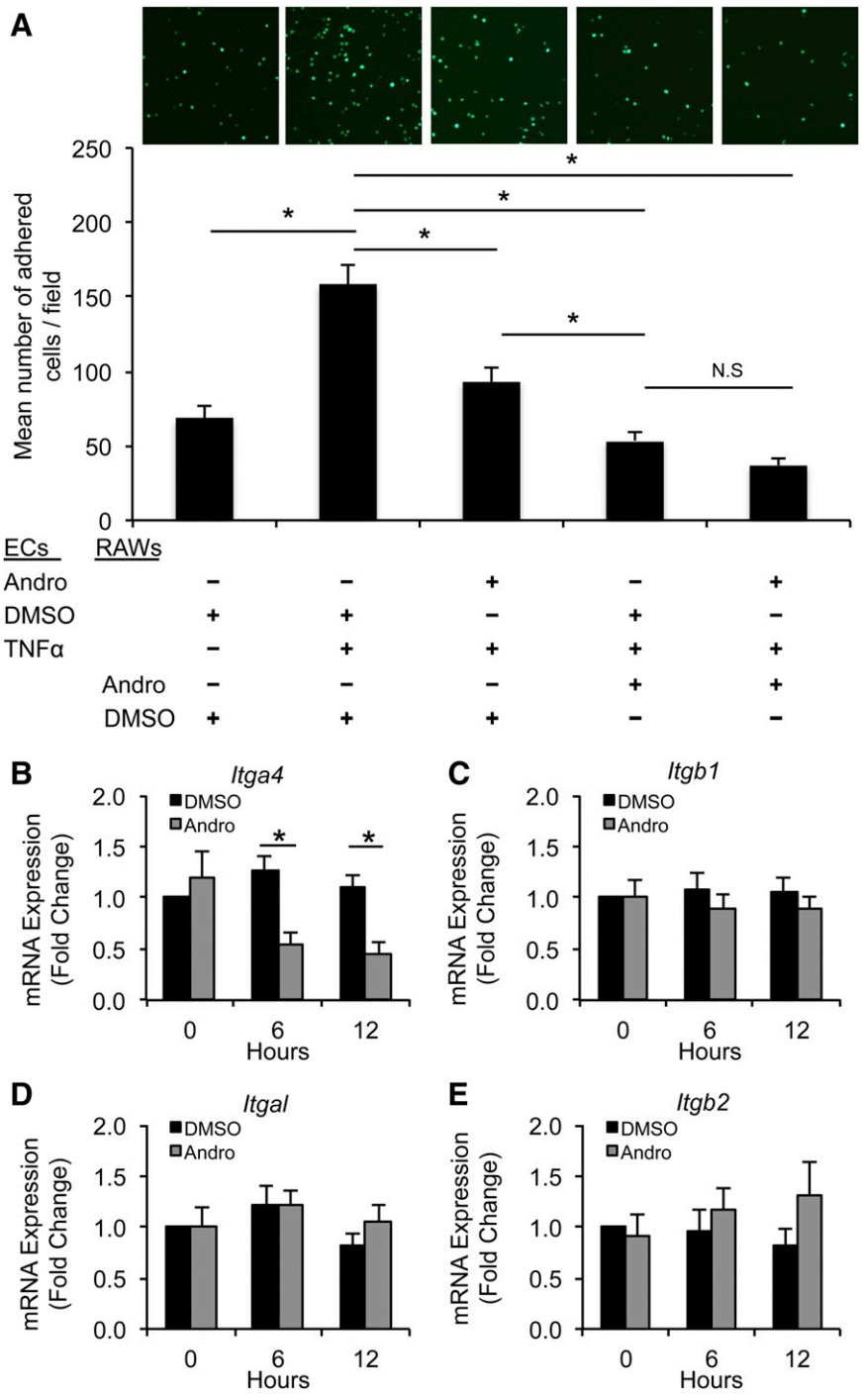

Fig. 5. Andro reduces the adherence of monocytes/macrophages to ECs. (A) Fluorescently labeled RAW264.7 cells, pretreated with Andro (15 μM) or DMSO, were incubated with TNFα-treated (10 ng/ml) ECs. After washing vigorously, adhered RAW264.7 cells were imaged (upper panel) and quantified (lower panel). Data are expressed as the mean number of adhered cells/field ± S.E.M. ($n = 4$; *$P < 0.05$, one-way analysis of variance). (B–E) RAW264.7 cells were treated with or without Andro (15 μM) or solvent for the indicated time. mRNA expression of α4 (B), β1 (C), αL (D), and β2 (E) integrins was analyzed by quantitative real-time PCR. All values represent the mean ± S.E.M. ($n = 4$–6; *$P < 0.05$, one-way analysis of variance). N.S., not significant.

post-translational modifications of p65, such as phosphorylation, influence its dimerization, DNA binding, and transcriptional activity, and are recognized as an alternative mechanism leading to NF-κB activation (Oeckinghaus and Ghosh, 2009). The effect of Andro on NF-κB activation appears to depend on the cell type and stimulus. In collagen-stimulated platelets, Andro affects NF-κB at IκB degradation (Lu et al., 2012). In SMCs, Hsieh et al. reported that Andro suppressed LPS/interferon-γ–induced p65 nuclear translocation, p65 phosphorylation, and DNA binding activity, but not degradation of IκB (Hsieh et al., 2011). Consistent with their findings, we found that Andro decreased p65 phosphorylation at Ser536 in both TNFα-treated SMCs and LPS-treated RAWs. However, Andro did not significantly alter IκB degradation in either cell type. We speculate that this IκB-independent effect of Andro allows cells to maintain certain NF-κB–mediated antiapoptotic proteins, including Bcl-2, A1, and IAP. This notion may explain the low cytotoxicity of Andro that we and other groups observed (Xia et al., 2004; Wang et al., 2007; Hsieh et al., 2011).

The involvement of NF-κB in aneurysm pathophysiology is implicated by a markedly elevated NF-κB activity in biopsies of human aneurysmal tissues and a mouse model of AAA (Miyake et al., 2006, 2007). Using an antibody specific to the

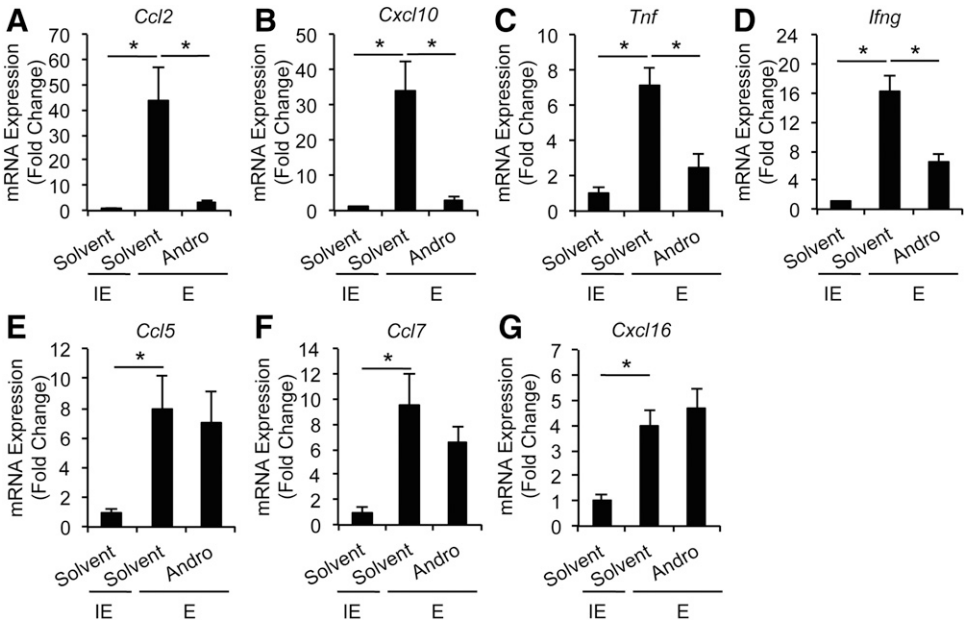

Fig. 6. Andro inhibits inflammatory cytokine expression in elastase-perfused aortic tissues. mRNA expression of Ccl2 (A), Cxcl10 (B), Tnf (C), Ifng (D), Ccl5 (E), Ccl7 (F), and Cxcl16 (G) in aorta of solvent- or Andro-treated animals 14 days after surgery was analyzed by quantitative real-time PCR. All values represent the mean ± S.E.M. (n = 3–8; $^*P < 0.05$, one-way analysis of variance). E, elastase; IE, inactivated elastase.

activated p65, we confirmed the prior reports and identified SMCs and macrophages as major cell types that harbor activated NF-κB. At 14 days post aneurysm induction, CD31-positive ECs remained sporadic in the elastase-treated aortic sections, likely due to endothelial damage during the perfusion procedure. The contribution of endothelial-specific NF-κB activation in aneurysm has been previously highlighted. Using a transgenic mouse line expressing dominant-negative IkBα selectively in ECs, Saito et al. (2013) demonstrated that selective NF-κB inhibition decreased macrophage infiltration and aneurysmal dilatation in the angiotensin II AAA model. The involvement of NF-κB in aneurysm development was also demonstrated by Nakashima et al. (2004), who inhibited the signaling pathway with an oligodeoxynucleotide decoy delivered to the aortic wall during the elastase perfusion procedure in rats. Given the established effects of Andro on the NF-κB pathway and the involvement of NF-κB in inflammation and aneurysm pathophysiology, it is plausible to attribute the antianeurysm effect of Andro to NF-κB inhibition. However, our data do not exclude other potential targets.

Beneficial effects of Andro have also been observed in several other experimental cardiovascular disease models, including restenosis, myocardial infarction, and hyperglycemia (Yu et al., 2003; Wang et al., 2007; Woo et al., 2008). Although these prior studies and our current work put Andro in a strong position as a drug candidate, caution should be taken when translating mouse work into clinical treatments. One concern relates to aneurysm modeling. Several murine

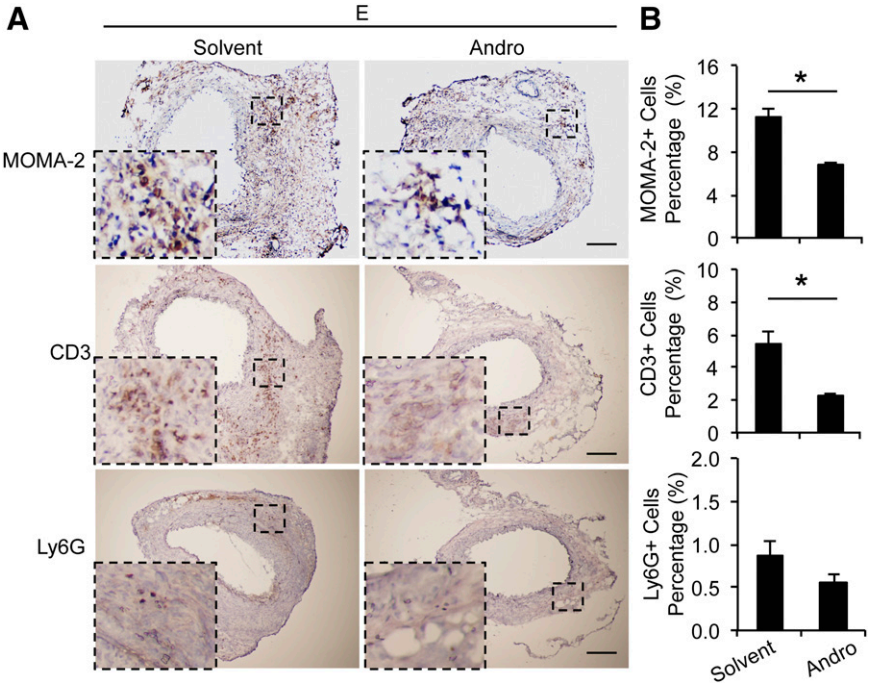

Fig. 7. Andro decreases infiltration of inflammatory cells in elastase-perfused aortic tissues. (A) Representative images of arterial sections immunohistochemically stained for MOMA-2 (a monocyte and macrophage marker), CD3 (a T cell marker), and Ly6G (a neutrophil marker). Higher-magnification views of boxed areas are shown at the lower-left corner. E, elastase. Scale bar = 200μm. (B) Quantification of inflammatory cell infiltration in aortic tissue is expressed as positive cells/nuclei. All values represent the mean ± S.E.M. (n = 6–10; $^*P < 0.05$, two-tailed Student's t test).

AAA models have been created with different strengths and weaknesses (Daugherty and Cassis, 2004). In this study, we used an elastase-induced AAA model, which recapitulates important pathologic features of human AAA, including SMC depletion, inflammation, and elastin degradation (Daugherty and Cassis, 2004; Thompson et al., 2006). However, it does not lead to AAA rupture, a major complication in human AAA (Nordon et al., 2011). Another concern in translation is drug toxicity. In this study, the mortality rate was 0 in both Andro-treated ($n = 7$) and solvent-treated ($n = 9$) groups. Consistent with prior studies, no differences in body weight and appearance were noticed between Andro- and solvent-treated mice. The safety of Andro is supported by a phase II clinical study of rheumatoid arthritis patients, which revealed that *A. paniculata* tablets containing 30 mg of andrographolide (three times a day for 14 weeks) were well tolerated and significantly more effective in reducing symptoms and serological parameters of the disease (Burgos et al., 2009). However, higher doses of Andro (4–6 mg/kg body weight, oral administration) may cause isolated cases of allergic reactions, tiredness, headache, pruritus/rash, diarrhea, nausea, metallic taste, bitter taste, and dry tongue (Coon and Ernst, 2004). Three additional clinical trials are currently being conducted to evaluate efficacy, safety, and tolerability of Andro in patients with multiple sclerosis and colorectal neoplasms.

In closing, our results indicate that Andro suppresses small aneurysm progression in an elastase-induced AAA mouse model. The therapeutic effect of Andro on AAA progression is achieved at least in part through inhibition of NF-κB activity, which subsequently diminishes production of inflammatory cytokines and chemokines as well as integrins. Thus, Andro may offer a safe and effective therapeutic strategy to slow disease progression in patients with small AAAs.

Acknowledgments

The authors thank Carmel Assa and Noel Phan for their intellectual inputs.

Authorship Contributions

Participated in research design: Ren, Z. Liu, Wang, B. Liu.

Conducted experiments: Ren, Z. Liu, Wang, Giles, Greenberg.

Contributed new reagents or analytic tools: Sheibani.

Performed data analysis: Ren, Z. Liu, Giles, Wang.

Wrote or contributed to the writing of the manuscript: Ren, Sheibani, Kent, B. Liu.

References

Aoki T, Kataoka H, Ishibashi R, Nozaki K, Egashira K, and Hashimoto N (2009) Impact of monocyte chemoattractant protein-1 deficiency on cerebral aneurysm formation. *Stroke* **40**:942–951.

Aoki T, Kataoka H, Shimamura M, Nakagami H, Wakayama K, Moriwaki T, Ishibashi R, Nozaki K, Morishita R, and Hashimoto N (2007) NF-kappaB is a key mediator of cerebral aneurysm formation. *Circulation* **116**:2830–2840.

Bown MJ, Sweeting MJ, Brown LC, Powell JT, and Thompson SG; RESCAN Collaborators (2013) Surveillance intervals for small abdominal aortic aneurysms: a meta-analysis. *JAMA* **309**:806–813.

Burgos RA, Hancke JL, Bertoglio JC, Aguirre V, Arriagada S, Calvo M, and Cáceres DD (2009) Efficacy of an Andrographis paniculata composition for the relief of rheumatoid arthritis symptoms: a prospective randomized placebo-controlled trial. *Clin Rheumatol* **28**:931–946.

Clowes AW, Clowes MM, Fingerle J, and Reidy MA (1989) Kinetics of cellular proliferation after arterial injury. V. Role of acute distension in the induction of smooth muscle proliferation. *Lab Invest* **60**:360–364.

Coon JT and Ernst E (2004) Andrographis paniculata in the treatment of upper respiratory tract infections: a systematic review of safety and efficacy. *Planta Med* **70**:293–298.

Curci JA and Thompson RW (2004) Adaptive cellular immunity in aortic aneurysms: cause, consequence, or context? *J Clin Invest* **114**:168–171.

Daugherty A and Cassis LA (2004) Mouse models of abdominal aortic aneurysms. *Arterioscler Thromb Vasc Biol* **24**:429–434.

Dua A, Kuy S, Lee CJ, Upchurch GR, Jr, and Desai SS (2014) Epidemiology of aortic aneurysm repair in the United States from 2000 to 2010. *J Vasc Surg* **59**: 1512–1517.

Eliason JL, Hannawa KK, Ailawadi G, Sinha I, Ford JW, Deogracias MP, Roelofs KJ, Woodrum DT, Ennis TL, and Henke PK, et al. (2005) Neutrophil depletion inhibits experimental abdominal aortic aneurysm formation. *Circulation* **112**:232–240.

Filardo G, Powell JT, Martinez MA, and Ballard DJ (2012) Surgery for small asymptomatic abdominal aortic aneurysms. *Cochrane Database Syst Rev* **3**: CD001835.

GBD 2013 Mortality and Causes of Death Collaborators (2015) Global, regional, and national age-sex specific all-cause and cause-specific mortality for 240 causes of death, 1990-2013: a systematic analysis for the Global Burden of Disease Study 2013. *Lancet* **385**:117–171.

Handa SS and Sharma A (1990) Hepatoprotective activity of andrographolide from Andrographis paniculata against carbontetrachloride. *Indian J Med Res* **92**: 276–283.

Hsieh CY, Hsu MJ, Hsiao G, Wang YH, Huang CW, Chen SW, Jayakumar T, Chiu PT, Chiu YH, and Sheu JR (2011) Andrographolide enhances nuclear factor-kappaB subunit p65 Ser536 dephosphorylation through activation of protein phosphatase 2A in vascular smooth muscle cells. *J Biol Chem* **286**:5942–5955.

Ip JE, Wu Y, Huang J, Zhang L, Pratt RE, and Dzau VJ (2007) Mesenchymal stem cells use integrin beta1 not CXC chemokine receptor 4 for myocardial migration and engraftment. *Mol Biol Cell* **18**:2873–2882.

Jayakumar T, Hsieh CY, Lee JJ and Sheu JR (2013) Experimental and clinical pharmacology of andrographis paniculata and its major bioactive phytoconstituent andrographolide. Evid Based Complement Alternat Med **2013**:846740.

Jayaraman T, Paget A, Shin YS, Li X, Mayer J, Chaudhry H, Niimi Y, Silane M, and Berenstein A (2008) TNF-alpha-mediated inflammation in cerebral aneurysms: a potential link to growth and rupture. *Vasc Health Risk Manag* **4**:805–817.

Jiang CG, Li JB, Liu FR, Wu T, Yu M, and Xu HM (2007) Andrographolide inhibits the adhesion of gastric cancer cells to endothelial cells by blocking E-selectin expression. *Anticancer Res* **27** (4B):2439–2447.

Kent KC (2014) Clinical practice. Abdominal aortic aneurysms. *N Engl J Med* **371**: 2101–2108.

Lengfeld J, Wang Q, Zohlman A, Salvarezza S, Morgan S, Ren J, Kato K, Rodriguez-Boulan E, and Liu B (2012) Protein kinase C δ regulates the release of collagen type I from vascular smooth muscle cells via regulation of Cdc42. *Mol Biol Cell* **23**:1955–1963.

Li PF, Dietz R, and von Harsdorf R (1997) Reactive oxygen species induce apoptosis of vascular smooth muscle cell. *FEBS Lett* **404**:249–252.

Liu Z, Morgan S, Ren J, Wang Q, Annis DS, Mosher DF, Zhang J, Sorenson CM, Sheibani N, and Liu B (2015) Thrombospondin-1 (TSP1) contributes to the development of vascular inflammation by regulating monocytic cell motility in mouse models of abdominal aortic aneurysm. *Circ Res* **117**:129–141.

Liu Z, Wang Q, Ren J, Assa CR, Morgan S, Giles J, Han Q, and Liu B (2014) Murine abdominal aortic aneurysm model by orthotopic allograft transplantation of elastase-treated abdominal aorta. *J Vasc Surg* DOI: S0741-5214(14)01000-3 [published ahead of print].

Longo GM, Xiong W, Greiner TC, Zhao Y, Fiotti N, and Baxter BT (2002) Matrix metalloproteinases 2 and 9 work in concert to produce aortic aneurysms. *J Clin Invest* **110**:625–632.

Lu CY, Yang YC, Li CC, Liu KL, Lii CK, and Chen HW (2014) Andrographolide inhibits TNFα-induced ICAM-1 expression via suppression of NADPH oxidase activation and induction of HO-1 and GCLM expression through the PI3K/Akt/Nrf2 and PI3K/Akt/AP-1 pathways in human endothelial cells. *Biochem Pharmacol* **91**:40–50.

Lu WJ, Lin KH, Hsu MJ, Chou DS, Hsiao G, and Sheu JR (2012) Suppression of NF-κB signaling by andrographolide with a novel mechanism in human platelets: regulatory roles of the p38 MAPK-hydroxyl radical-ERK2 cascade. *Biochem Pharmacol* **84**:914–924.

MacTaggart JN, Xiong W, Knispel R, and Baxter BT (2007) Deletion of CCR2 but not CCR5 or CXCR3 inhibits aortic aneurysm formation. *Surgery* **142**:284–288.

Miyake T, Aoki M, Masaki H, Kawasaki T, Oishi M, Kataoka K, Ogihara T, Kaneda Y, and Morishita R (2007) Regression of abdominal aortic aneurysms by simultaneous inhibition of nuclear factor kappaB and ets in a rabbit model. *Circ Res* **101**: 1175–1184.

Miyake T, Aoki M, Nakashima H, Kawasaki T, Oishi M, Kataoka K, Tanemoto K, Ogihara T, Kaneda Y, and Morishita R (2006) Prevention of abdominal aortic aneurysms by simultaneous inhibition of NFkappaB and ets using chimeric decoy oligonucleotides in a rabbit model. *Gene Ther* **13**:695–704.

Moehle CW, Bhamidipati CM, Alexander MR, Mehta GS, Irvine JN, Salmon M, Upchurch GR, Jr, Kron IL, Owens GK, and Ailawadi G (2011) Bone marrow-derived MCP1 required for experimental aortic aneurysm formation and smooth muscle phenotypic modulation. *J Thorac Cardiovasc Surg* **142**:1567–1574.

Nakashima H, Aoki M, Miyake T, Kawasaki T, Iwai M, Jo N, Oishi M, Kataoka K, Ohgi S, and Ogihara T, et al. (2004) Inhibition of experimental abdominal aortic aneurysm in the rat by use of decoy oligodeoxynucleotides suppressing activity of nuclear factor kappaB and ets transcription factors. *Circulation* **109**:132–138.

National Research Council (2011) Guide for the Care and Use of Laboratory Animals. 8th edition. Washington (DC): National Academies Press, US.

Nordon IM, Hinchliffe RJ, Loftus IM, and Thompson MM (2011) Pathophysiology and epidemiology of abdominal aortic aneurysms. *Nat Rev Cardiol* **8**:92–102.

Oeckinghaus A and Ghosh S (2009) The NF-kappaB family of transcription factors and its regulation. *Cold Spring Harb Perspect Biol* **1**:a000034.

Pyo R, Lee JK, Shipley JM, Curci JA, Mao D, Ziporin SJ, Ennis TL, Shapiro SD, Senior RM, and Thompson RW (2000) Targeted gene disruption of matrix metalloproteinase-9 (gelatinase B) suppresses development of experimental abdominal aortic aneurysms. *J Clin Invest* **105**:1641–1649.

Ren J, Wang Q, Morgan S, Si Y, Ravichander A, Dou C, Kent KC, and Liu B (2014) Protein kinase C-δ (PKCδ) regulates proinflammatory chemokine expression through cytosolic interaction with the NF-κB subunit p65 in vascular smooth muscle cells. *J Biol Chem* **289**:9013–9026.

Saito T, Hasegawa Y, Ishigaki Y, Yamada T, Gao J, Imai J, Uno K, Kaneko K, Ogihara T, and Shimosawa T, et al. (2013) Importance of endothelial NF-κB signalling in vascular remodelling and aortic aneurysm formation. *Cardiovasc Res* **97**:106–114.

Shimizu K, Mitchell RN, and Libby P (2006) Inflammation and cellular immune responses in abdominal aortic aneurysms. *Arterioscler Thromb Vasc Biol* **26**:987–994.

Si Y, Ren J, Wang P, Rateri DL, Daugherty A, Shi XD, Kent KC, and Liu B (2012) Protein kinase C-delta mediates adventitial cell migration through regulation of monocyte chemoattractant protein-1 expression in a rat angioplasty model. *Arterioscler Thromb Vasc Biol* **32**:943–954.

Su X, Sorenson CM, and Sheibani N (2003) Isolation and characterization of murine retinal endothelial cells. *Mol Vis* **9**:171–178.

Thompson RW, Curci JA, Ennis TL, Mao D, Pagano MB, and Pham CT (2006) Pathophysiology of abdominal aortic aneurysms: insights from the elastase-induced model in mice with different genetic backgrounds. *Ann N Y Acad Sci* **1085**:59–73.

Thompson RW, Holmes DR, Mertens RA, Liao S, Botney MD, Mecham RP, Welgus HG, and Parks WC (1995) Production and localization of 92-kilodalton gelatinase in abdominal aortic aneurysms. An elastolytic metalloproteinase expressed by aneurysm-infiltrating macrophages. *J Clin Invest* **96**:318–326.

Vorkapic E, Lundberg AM, Mäyränpää MI, Eriksson P, and Wågsäter D (2015) TRIF adaptor signaling is important in abdominal aortic aneurysm formation. *Atherosclerosis* **241**:561–568.

Wang Q, Liu Z, Ren J, Morgan S, Assa C, and Liu B (2015) Receptor-interacting protein kinase 3 contributes to abdominal aortic aneurysms via smooth muscle cell necrosis and inflammation. *Circ Res* **116**:600–611.

Wang Q, Ren J, Morgan S, Liu Z, Dou C, and Liu B (2014) Monocyte chemoattractant protein-1 (MCP-1) regulates macrophage cytotoxicity in abdominal aortic aneurysm. *PLoS One* **9**:e92053.

Wang YJ, Wang JT, Fan QX, and Geng JG (2007) Andrographolide inhibits NF-kappaBeta activation and attenuates neointimal hyperplasia in arterial restenosis. *Cell Res* **17**:933–941.

Woo AY, Waye MM, Tsui SK, Yeung ST, and Cheng CH (2008) Andrographolide up-regulates cellular-reduced glutathione level and protects cardiomyocytes against hypoxia/reoxygenation injury. *J Pharmacol Exp Ther* **325**:226–235.

Xia YF, Ye BQ, Li YD, Wang JG, He XJ, Lin X, Yao X, Ma D, Slungaard A, and Hebbel RP, et al. (2004) Andrographolide attenuates inflammation by inhibition of NF-kappa B activation through covalent modification of reduced cysteine 62 of p50. *J Immunol* **173**:4207–4217.

Yu BC, Hung CR, Chen WC, and Cheng JT (2003) Antihyperglycemic effect of andrographolide in streptozotocin-induced diabetic rats. *Planta Med* **69**: 1075–1079.

Zhu T, Wang DX, Zhang W, Liao XQ, Guan X, Bo H, Sun JY, Huang NW, He J, and Zhang YK, et al. (2013) Andrographolide protects against LPS-induced acute lung injury by inactivation of NF-κB. *PLoS One* **8**:e56407.

Address correspondence to: Dr. Bo Liu, Department of Surgery, University of Wisconsin–Madison, 1111 Highland Avenue, WIMR 5137, Madison, WI 53705. E-mail: liub@surgery.wisc.edu